Available online at www.sciencedirect.com
ScienceDirect
International Journal of Heat and Mass Transfer 50 (2007) 502–512
International Journal of HEAT and MASS TRANSFER
www.elsevier.com/locate/ijhmt

R-134a spray dynamics and impingement cooling in the non-boiling regime

Shou-Shing Hsieh *, Chi-Hsun Tien

Department of Mechanical and Electro-Mechanical Engineering, National Sun Yat-Sen University, Kaohsiung 80424, Taiwan, ROC

Received 22 July 2005; received in revised form 28 July 2006
Available online 28 September 2006

Abstract

R-134a spray as it impinges on the flat endplate of a circle is studied experimentally. In order to optimize R-134a spray cooling efficiency, a detailed characterization and understanding of liquid spray formation is essentially needed. An optical image system was used to quantify the spray flow structure. LDV measurements were used to characterize the local velocity /and velocity fluctuation distribution from a commercial available nozzle in both axial and radial directions. The radial velocity are found to be the largest at the outer edges of the spray, and they continuously decrease across the spray toward the center axis; while the corresponding axial velocity is the maximum there. Moreover, spray heat transfer in non-boiling regime was shown to be dependent on the velocity of the impinging spray in terms of Weber number and other related parameters which are in good agreement with those of previous studies.

1. Introduction

The fluid mechanics of drop impingement with surfaces are of importance in a variety of applications such as spray cooling, combustion, and spray drying [1–5]. As with many phenomena, the full characterization of liquid droplets in sprays while in-flight is a very important engineering issue. The information of droplets velocity while in-flight will assist in the characterization and further optimization of the droplet size in spray cooling application. The major difficulty in determining the size and velocity of the in-flight small droplets is the lack of a suitable non-intrusive means to measure them accurately. Ingebo [6] made drop size measurements of the spray from a jet impinging on splash-plate by using photographic techniques with the following empirical equation for the mean diameter of the drops in quiescent air

$$d = \frac{d_o}{cRe_o} \tag{1}$$

where $c = 2.8 \times 10^{-4}$ and d_o is the jet nozzle diameter and $Re_o = \rho u_j d_o/\mu_j$ is the liquid jet Reynolds number with μ_j being the liquid jet viscosity.

There have been several studies on water sprays, from which empirical correlation of various spray characteristics have been developed. Elkotb [7] proposed correlations to estimate the Sauter mean diameter (SMD) of droplets produced by plain orifice atomizers. Zhou et al. [8] studied the influence of gas and liquid flow rates on the droplet sizes and velocities produced by a linear atomizer. Two-component phase doppler interferometer (PDI) is applied to a water spray to quantify the spray characteristics as a function of operating conditions. In addition to the conventional spray cooling the growth of laser technology and the relative non-invasiveness of dermatological laser surgery has led to a dramatic increase of cutaneous laser producers over the past two decades [5]. Laser radiation is correctly used for hair removal and port wine stain birthmarks. This is related an upcoming area known as cryogen spray cooling (CSC). Regarding cryogenic spray, Ingebo [9] investigated the effects of gas temperature, gas properties, and vaporization on droplet size of sprays produced by two fluid type nozzles, where a high velocity gas was

* Corresponding author. Tel.: +886 07 5252000x4215; fax: +886 07 5254215.
E-mail address: sshsieh@mail.nsysu.edu.tw (S.-S. Hsieh).

0017-9310/$ - see front matter © 2006 Elsevier Ltd. All rights reserved.
doi:10.1016/j.ijheatmasstransfer.2006.07.023

Nomenclature

d_o	spray nozzle diameter, mm	r	r ordinate, mm
d_{32}	Sauter mean diameter (SMD), mm	T_l	spray liquid temperature, °C
G	mass flux, kg/m^2 s	T_s	impingement plate surface temperature, °C
H	the distance from spray exit to the target plate, mm	u	mean axial velocity, m/s
		u_e	spray exit centerline velocity, m/s
h	local heat transfer coefficient, W/m^2 °C	u_o	spray centerline mean velocity, m/s
k_l	thermal conductivity of spray liquid, W/m °C	u_p	spray impact velocity, m/s
k_{ss}	thermal conductivity of stainless steel plate, W/m °C	u'	axial velocity fluctuation, m/s
		v	mean radial velocity, m/s
$\bar{h}$	average heat transfer coefficient, W/m^2 °C	v'	radial velocity fluctuation, m/s
L	side length of the square impingement plate, mm	We	spray Weber number, $\rho u_p^2 d_{32}/\sigma$
Nu_L	Nusselt number, hL/k	z	distance from the nozzle, mm
P	pressure, Pa	ΔT	$T_s - T_l$, °C
ΔP	pressure drop, Pa	μ	liquid dynamic viscosity, Pa s
q_s	average surface heat flux, W/m^2	ρ	liquid density, kg/m^3
Re_0	spray exit Reynolds number, $u_e d_o/v$	σ	surface tension, N/m
Re^*	modified Reynolds number, Gd_o/μ		

used to atomize the liquid cryogen. Some correlations were developed for mean droplet diameters of cryogen sprays in terms of gas mass flux, cryogen and gas properties, and nozzle geometry. All results mentioned above indicate that the droplet size and spatial distribution are critical to the optimization of process parameters. Moreover, the droplet velocity is also important because it determines the droplet flight time and heat transfer characteristics. Therefore, characterization of droplet size and velocity distribution may provide feedback for control of operating variables in liquid spraying.

Impingement heat transfer has been used extensively in industry because of the high cooling rates it provides. Most of papers published [10,11] falls into the category in which the spray droplets impact a heated surface and then, spread on the surface and evaporate, removing large amounts of energy at low temperatures due to the latent heat of evaporation in addition to substantial convection effects. However, there has been little work [12] examining the cooling capacities of non-boiling sprays impinging onto a heated surface.

There has been an increased demand for new technique capable of removing high heat fluxes and such demands will continue to increase in the future. Among these technique, spray cooling is one of the most notable methods to remove high heat flux. It is long recognized [13] that spray cooling with phase change has been demonstrated to be a powerful method to remove high heat flux (>1000 W/cm^2) from surfaces with a considerable low wall superheat.

In addition to the above discussion, there seems quite a few papers [13,14] dealing with the spray cooling topics by using refrigerants as working mediums especially for non-CFC refrigerants and their associated applications in refrigerations and air conditioning industry. It is essentially necessary to complement the existing data of spray cooling by providing the related information and document for non-CFC refrigerants at this stage.

As stated previously, it appears that there is a very limited knowledge base on spray impingement cooling of surfaces for situations where the surface temperature is below the boiling point of liquid. Only a few experimental studies have been reported and differences in the results reported by different investigators are inconsistently large [15]. In view of the foregoing discussion, this paper presents a detailed investigation of the impinging spray atomization, spray droplet dynamics, and spray impingement heat transfer. Spray characteristics such as mean velocity, and volume flux will be measured at different locations in the spray as well as the target wall temperature will be measured. The objective of the study is to investigate pre-impingement processes, flow structure, and cooling capacity of the plate as related to spray cooling. More specifically, this work will examine in detail what happens to droplet while traveling in a quiescent air environment prior to hit the target surface. The effects of the impinging spray jet velocity on the spray characteristics will also be studied. Furthermore, single-phase spray impingement cooling measurements will also be conducted and results will be presented and discussed.

2. Experimental

Fig. 1 is a schematic of the apparatus used for spray cooling experiments. It consists of a nozzle-spray system, and target surface which were housed in a stainless steel cylindrical chamber (250 mm long × 200 mm dia.) with a glass sheet top ceiling. A circular sight glass was made in front of the chamber with a dimension of ID 140 mm, and centered at the 100 mm below the top of the test

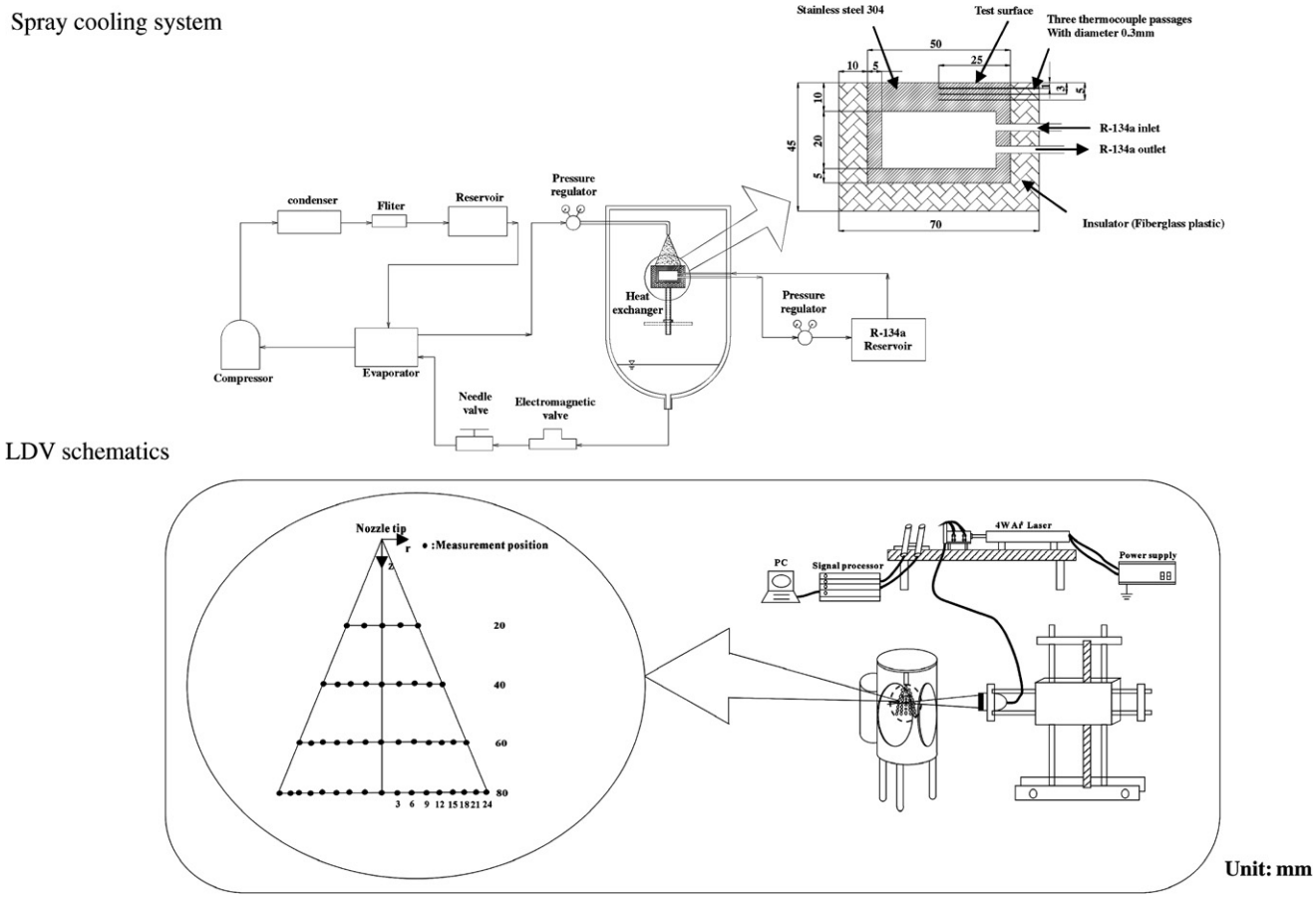

Fig. 1. Schematics of the present R-134a spray cooling system.

chamber. The experiments were conducted using R-134a at 12, 14, and 16 °C, respectively as a test liquid ($\rho = 1232$ kg/m^3, $\mu = 2.3 \times 10^{-4}$ Pa s, $\sigma = 9.2 \times 10^{-3}$ N/m). The spray is locally characterized by droplet diameter, droplet velocity and volume flux density. This information is obtained by a spatially resolving optical imaging system and LDV measurements at 20, 40, 60, and 80 mm downstream of the nozzle exit when no further droplet breakup occurs. Photos of the flow structures were taken using a flashlamp incorporated with a progressive-scan camera. The spark has duration time of approximately 5 μs which is sufficiently short to freeze the motion of liquid phase (see Table 1).

Table 1
Relevant geometric and working parameters and variables of Sauter mean diameter

LDV flow measurements			
The diameter of test section (mm)	80		
Test surface to nozzle distance, H (mm)	90		
Spray nozzle diameter, d_0 (mm)	0.51		
Working medium	R-134a		
Pressure difference, ΔP (MPa)	0.3	0.5	0.7
Sauter mean diameter, d_{32} (μm)	50	35	28
Weber number, We	70	76	85
Heat transfer measurements			
Chamber saturation temperature (°C)	25		
Chamber pressure	0.65 MPa		
R-134a spray temperature at the nozzle exit (°C)	12, 14, 16		
Impingement surface (target surface) temperature (°C)	20		
Spray mass flux (target surface), G (kg/m^2 s)	1.33–1.40		
Heat flux, q_s (W/m^2)	58,885–115,386		

2.1. Liquid supply/heat removal system

R-134a delivery systems used in this study consisted of

(a) a commercially available nozzle (TG Spray Co. Ltd.) with a diameter of 0.51 mm was used to achieve different values (1.33–1.40 kg/m^2 s) of R-134a mass flux sprayed onto a flat plate. The spray nozzle located normal to and directly above the center of the upward-facing flat plate. The nozzle provided presumably uniform coverage and the manufacturer-specified droplet Sauter mean diameter was specified,
(b) a liquid supply system with an orifice diameter of 4 mm.

The flat plate was placed at a distance $z = 90$ from the nozzle tip, centered along the axis of the spray. The target

wall temperature was fixed at 20 °C with three different spray jet exit temperatures of 12, 14, and 16 °C to observe the heat removal rate in the non-boiling regime. Three K type, 40 gauge, ceramic-encased, thermocouples were embedded along the centerline underneath the flat plate which were positioned at 1 mm, 3 mm, and 5 mm along the centerline to measure the heat transfer through the impingement surface. Schematic of heater design and test section can be found in [13].

To obtain a steady state measurement, all temperature measurements were taken at least 300 s after onset of spraying or any change in the heat impact. A series of measurements was performed while changing Weber number, which can be achieved by adjusting the mass flux. The present heat transfer rate can be calculated based on the convective boundary condition at the target plate, which is

$$k_{ss}\left(\frac{dT}{dx}\right)_{x=0^+} = h(T_s - T_c) \tag{2}$$

Here, k_{ss} is the thermal conductivity of stainless steel (SS304) plate, $T_s = T(x = 0^+)$ is wall temperature of the target plate, and T_c is the average temperature of spray liquid layer on the target surface. The temperature gradients, $(dT/dx)^+_{x=0}$ at the surface temperature of the stainless steel plate, T_s, were determined by extrapolation of best fit through temperature measurements acquired simultaneously along the thickness of the plate.

Average heat transfer coefficient for the spray cooling was determined for each experimental run from the following relation:

$$\bar{h} = q''_s/(T_s - T_l) \tag{3}$$

where the average surface heat flux q''_s, obtained from Eq. (2), and impingement surface temperature T_s were determined from the parabolic curve fit of centerline temperature in the stainless steel surface. (i.e. Eq. (2)) The spray liquid temperature T_l was measured with a thermocouple at the nozzle exit. The present heat leak was negligible because it was carefully controlled.

2.2. Spray mass flux measurements

The spray mass flux at the flat plate was calculated for different pressure drop by replacing the test surface with a section of copper tubing whose internal diameter was the same as the diameter of the surface area as well as with the tubing pressure identical to the chamber pressure, and recording the volume of liquid flowing into the tubing within a known time period. These experiments were repeated at least three times for each run. The measurements above were estimated to be accurate within ±6%.

2.3. Spray velocity

The spatial velocity characteristics of liquid spray impinging at 90° on unheated walls were studied by using LDV measurements. The measuring locations corresponding to representative regions of the downstream spray which indicate all the measurement positions were located outside the spray impingement area to ensure that all the droplets associated with the incident free spray were considered in this study. Also shown in Fig. 1 is the present LDV measurement system. The present system is a commercial two color, four beam DANTEC fringe-type LDV system, operated in the backward scatter mode with the general layout shown in Fig. 1 which is similar to that of Hsieh et al. [16]. Standard DANTEC 55x modular optics and a model Stabilite 2016 4W Spectra Physics Ar^+ laser are mounted on a two-dimensional, traversing system. Two separate LDV channels are formed by use of color separation of beams with wavelengths 514.5 nm (green light) and 488.0 nm (blue light). These two beams form orthogonal fringes by means of a standard DANTEC two channel optical train. These two sets of fringes allow the simultaneous measurement of two orthogonal velocity components. The transverse velocity component is measured using the 488.0 nm beam, while the 514.2 nm beam measures a streamwise velocity component. A combined counter-type signal processor (Dantec model 57H00) with functions of counter, buffer interface and coincidence

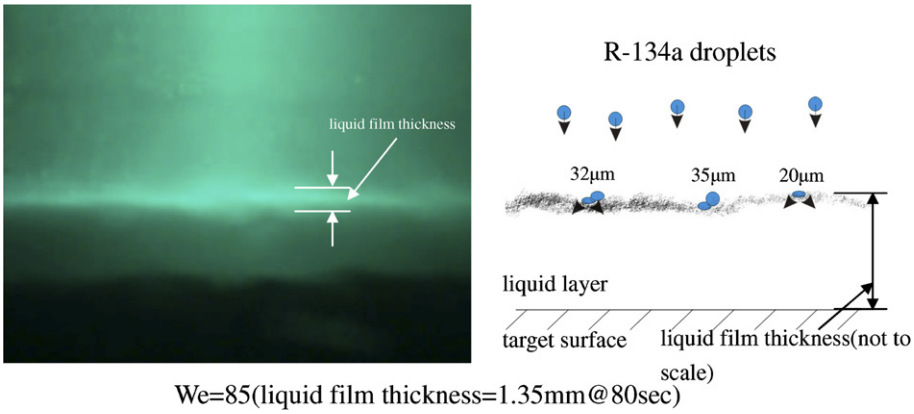

Fig. 2. Magnified (×5.2) images of the R-134a spray.

filter, which is interfaced with a LEO (Intel-486) PC in the direct access mode, was employed for data processing. Statistical data were based on a sample size of 320,000 measurements with a sampling frequency of approximately 400 samples/s, from which the time-averaged values were determined.

The digital value of the Doppler frequency shift f_D, the characteristic wavelength of the laser λ, and the half angle between the beams $\theta/2$ are translated to horizontal (streamwise) u and vertical (transverse) v velocity components, respectively, by the equation

$$u/\text{or } v = \frac{\lambda_{u/\text{or } v} f_D}{2\sin(\theta/2)} \tag{4}$$

Data were taken whenever a signal was validated. Moreover, the droplet frequency can be simultaneously measured.

3. Measurement considerations and errors estimation

Using the repeatability of measurements, the uncertainty in the estimation of the mean and fluctuating quantity was examined. In addition, various sources of uncertainty contribute to the random and system errors in the mean velocity measurements. These include index of refraction effects that alter the half angle between the beams and the optical probe volume location; velocity bias, filter bias, and velocity gradient broadening; and finite size

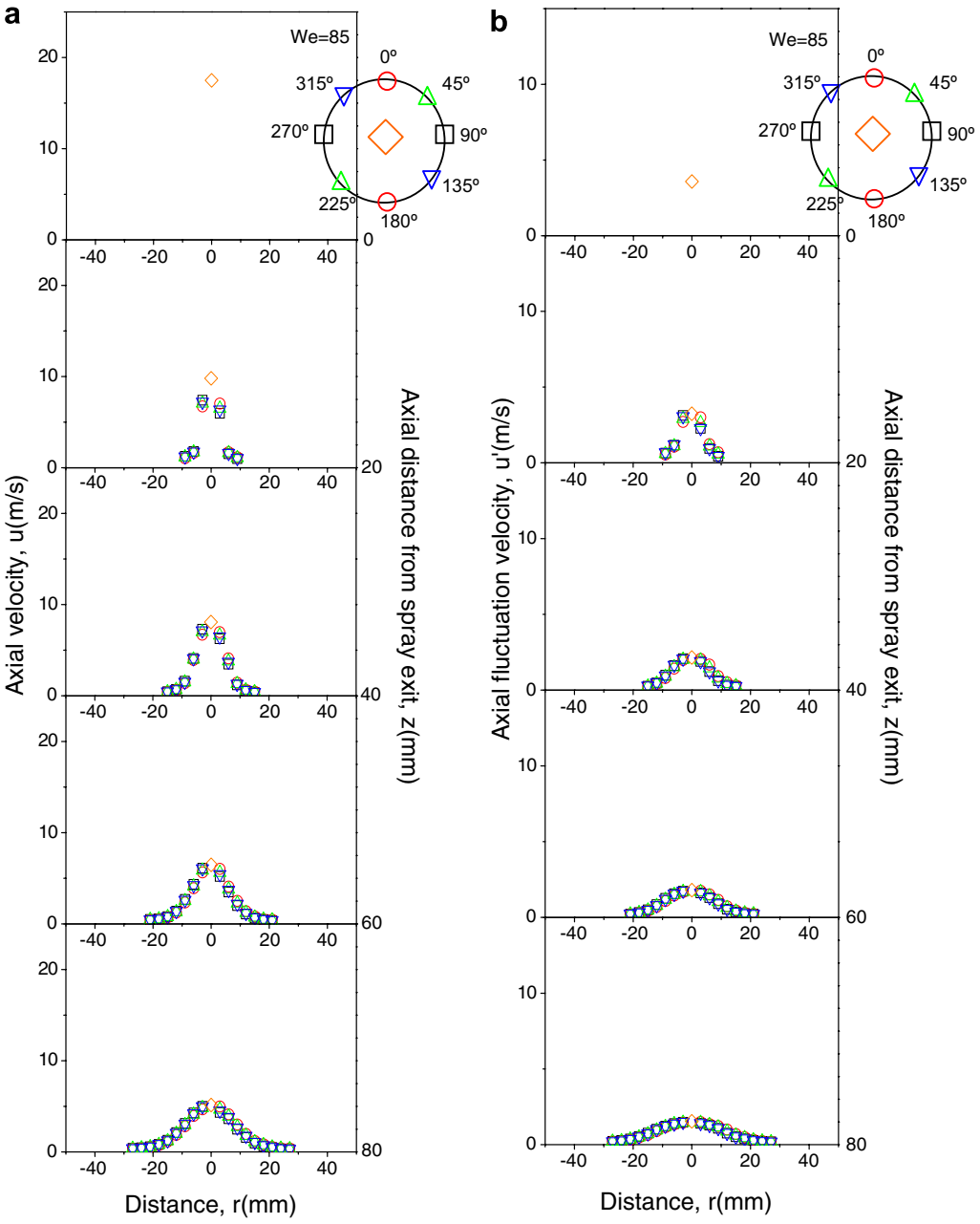

Fig. 3. Axial velocity and velocity fluctuation at $We = 85$.

of the data samples. The visual optical probe volume (640 μm × 760 μm) positioning uncertainty was kept less than ±0.002 mm by the careful determination of an initial reference location and using stepping motors with incremental steps equal to 50 μm. The uncertainty in the mean velocity measurements was found to be within ±8% based on the jet exit velocity, and with ±14% in the rms fluctuating velocity measurements based on the maximum turbulence intensity. The error in temperature difference between the spray and the impingement surface was estimated to be less than 8%. The typical heat flux between 0.06 and 0.12 MW/m^2 was found to be approximately ±12%.

4. Results and discussion

4.1. Spray jet flow visualization

From spray visualization, the cryogen exits the nozzle in a cone shaped fashion, resulting in finer atomization and widen slightly about 33 mm downstream at a spray span angle of 36°, 40° and 46° (not shown). For three different *We*, the overall spray shapes seem to be no significant differences in atomization. However, cryogen evaporation seems significant to share certain contribution on droplet reductions. These droplets experience stable coalescence following by fragmentation.

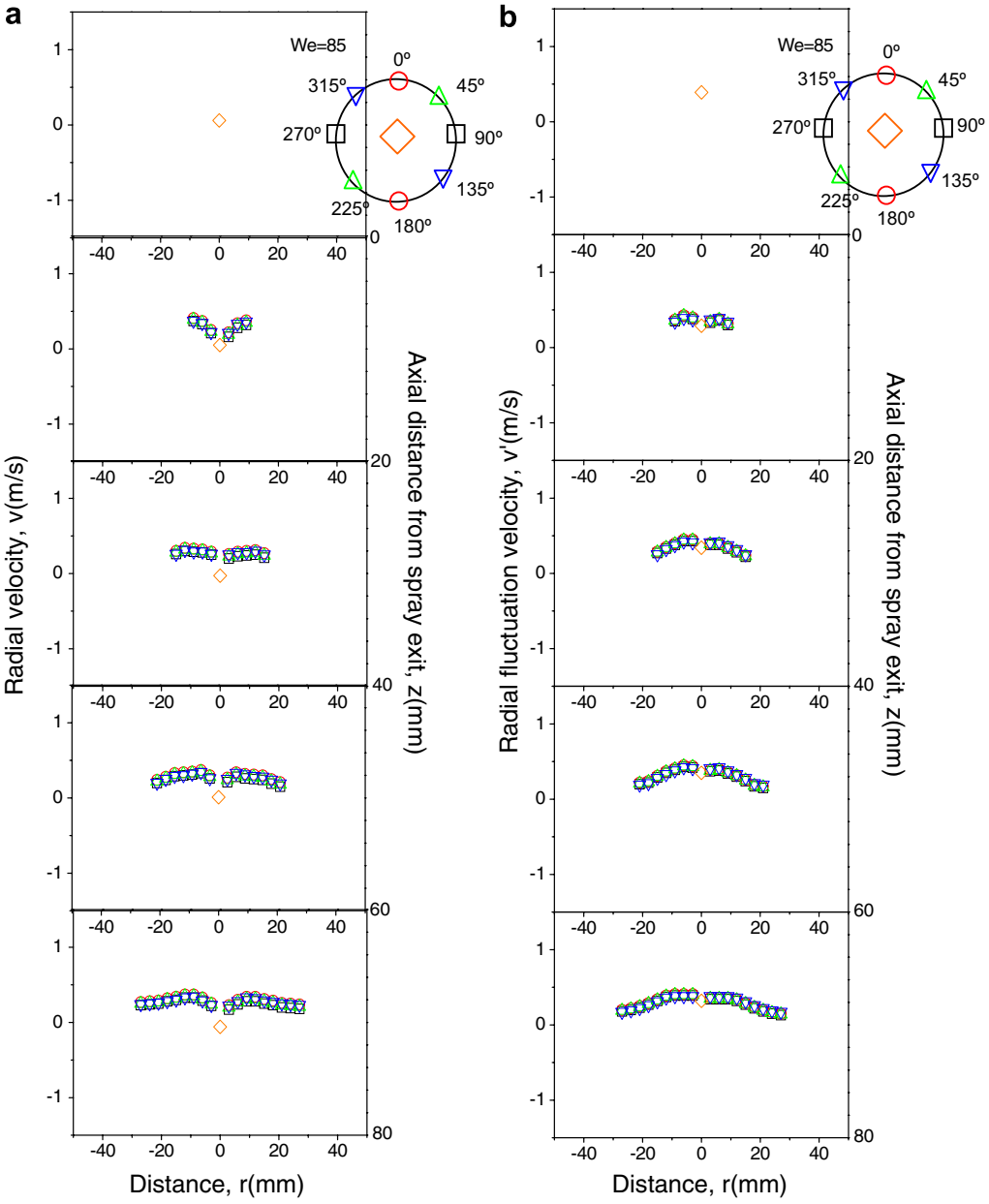

Fig. 4. Radial velocity and velocity fluctuation at $We = 85$.

It can be seen in Fig. 2 that the surface was almost completely wet by R-134a for all the cases under study. Fig. 2 shows one of the spray deposition conditions and the finely atomized sprays produced by the present nozzle on left and right column, respectively at $We = 85$. There seems a liquid layer blanketed the entire surface which are different from those found in [17] where quite a few dry spots appeared, likely due to a surface perturbation from either convective film instabilities or impact droplets. The liquid droplets impinge on the surface and join the liquid film. The thickness was found to increase with *We*. Basically, they coincided with the Sauter mean diameter (SMD) provided by nozzle suppliers. Thickness for spray impingement has been measured to be 0.93–1.35 mm through optical visualization with proper processing software. The very finest visible droplets were found especially for $We = 85$ and may be a result of droplet impacts directly from the spray. However, the intermediate size droplets ($We = 76$) that are much bigger than the very finest droplets ($We = 85$) are likely to be the result of the liquid film vaporizing (not shown). It is also possible due to colescence of smaller spray droplets. This situation becomes more noted as *We* increases. In fact, the present *We* of this study are not high ($\sim$77) but moderate. A relatively high Weber number corresponds to a larger volumetric flux, which would increase R-134a buildup and this would get the surface fully blanketed by liquid film and the layer becomes thicker as well.

4.2. Mean axial velocity and velocity fluctuation distribution

The velocity vector is proved to be symmetric with respect to the *z*-axis. Namely, it was found that the vector plots on each individual sector plane is azimuthal direction independent. The vector has the smallest magnitude at the outer edges of the spray with an increasing velocity at the spray axis as the spray proceeds downstream. The values of velocity vectors increase as *We* increases. Such an increase is quite a lot even though there is only a small increment in *We*. Also, spray cone angle gradually increases as *We* increases.

Fig. 3(a) represents the axial velocity profiles for different azimuthal angles of each 45° interval and jet centerline velocity at $We = 85$. The azimuthal instability does occur due to unequal velocity and it gets worse as *We* increases. However, such situation becomes less noted as the R-134a spray flies downstream. Generally, the velocity non-uniformity across the spray exhibits and become more parabolic velocity profiles was expected as the flow approaching the target at $z \cong 80$ mm from the nozzle exit. The centerline has a considerable higher velocity value with a lowest velocity at the outer edges of the spray /or the rims of the liquid sheet. In fact, this maximum velocity (i.e., spray centline velocity) would decrease along downstream.

Fig. 3(b) depicts the axial velocity fluctuations along the downstream distance at $We = 85$. These plots strongly indicate that the stability is across the spray where a noticeable velocity fluctuation exists at the outer edges of the spray and it becomes bigger while it travels across the spray until at the spray axis (centerline) where the velocity fluctuation has a maximum value. These happened to all *We*. However, with a higher *We*, indicating a higher spray exit velocity, e.g. $We = 85$, a more uniform velocity profile may not be obtained as compared to the rest cases of $We = 70$ and 76 (not shown). The u' had a maximum value of 4 m/s in the other region of the developing boundary layer at the spray centerline and at downstream 20 mm from the spray exit.

4.3. Mean radial velocity and velocity fluctuation distribution

Fig. 4(a) represents mean radial velocity profile across the liquid spray, unlike the axial velocity, the smallest

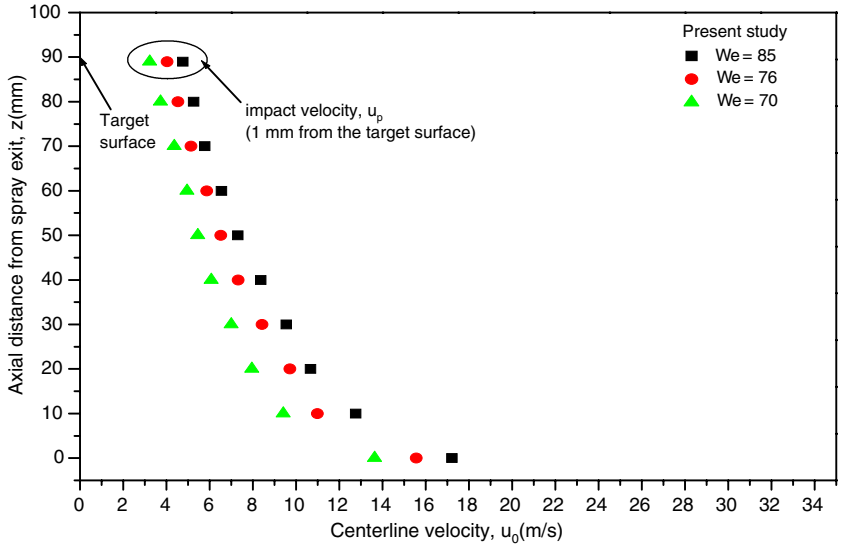

Fig. 5. Spray centerline velocity at $We = 70$, 76, and 85.

velocity happens at the outer edges of the spray and the velocity gradually increases until the spray axis approaches across the entire flow domain. The velocity has the minimum value at the spray axis. However, this situation becomes less noted as flow proceeds downstream. At that stage, this mixing becomes complete; i.e., the spray seems fully developed and the velocity becomes more flat and uniform.

Fig. 4(b) shows the radial velocity fluctuation distribution. The values seem large while the jet is developing as expected. The profiles become more uniform/flat as it flows downstream. Furthermore, the rim/outer edge becomes bigger as *We* increases. High values of v' with a lateral spread with increasing distance downstream from the nozzle exit were observed. In contrast, the radial velocity fluctuations in the outer region exhibited low values at the same locations as the axial component. The magnitude of peak of (v') was about one fourths of the peak (u') in the outer shear layer.

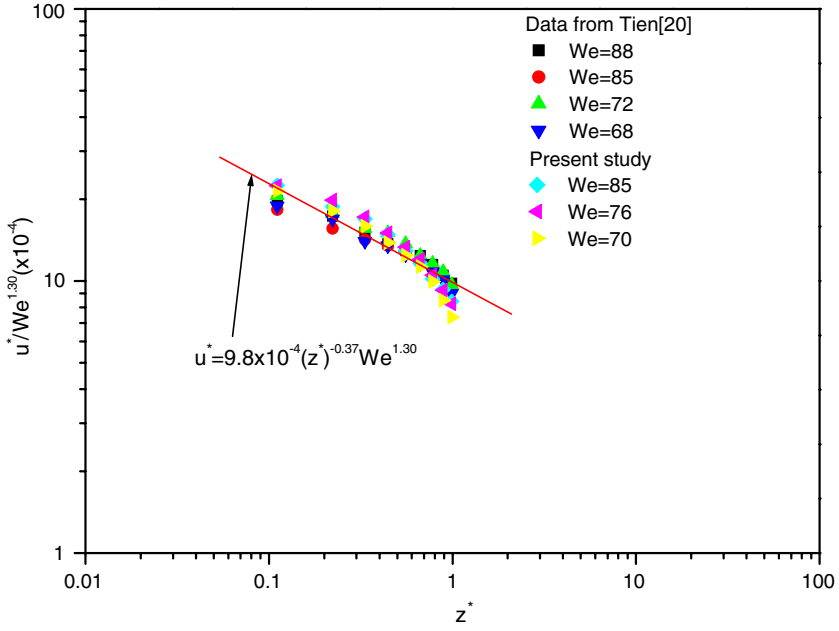

Fig. 6. z^* and *We* dependence on u^*.

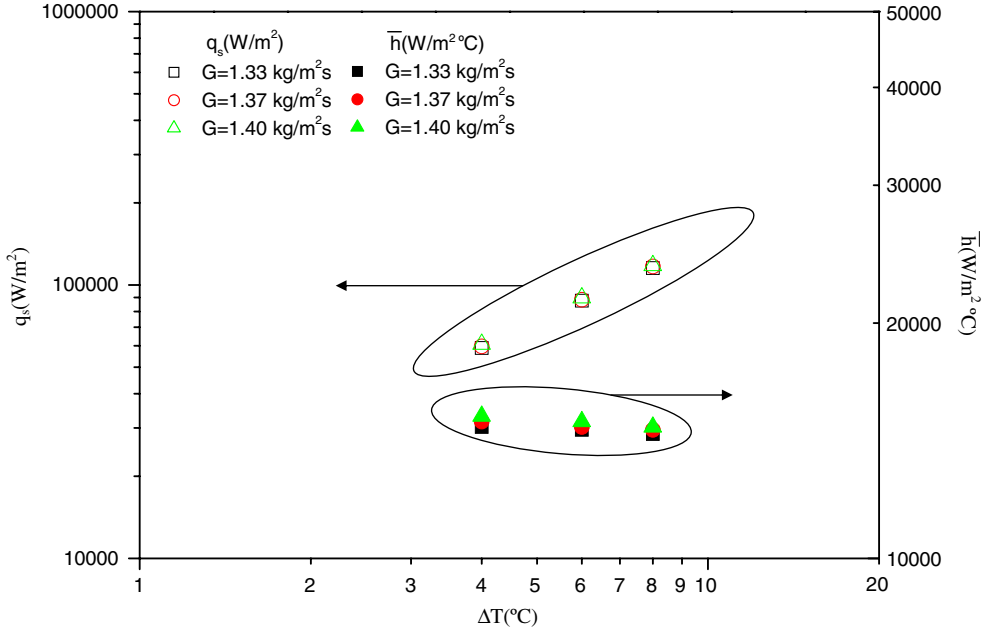

Fig. 7. q_s and $\bar{h}$ vs. $\Delta T(=T_s - T_l)$.

4.4. Average spray centerline velocity profiles and impact velocity

Fig. 5 shows the average spray centerline velocity along downstream distance with impact velocity at $We = 70$, 76, and 85, respectively. The impact velocity was measured at $z = 89$ mm away from the nozzle exit, which is very close to the target surface, $z = 90$ mm, from the nozzle exit. The velocity reductions were found to be similar to a conventional jet. However, the potential core region seems

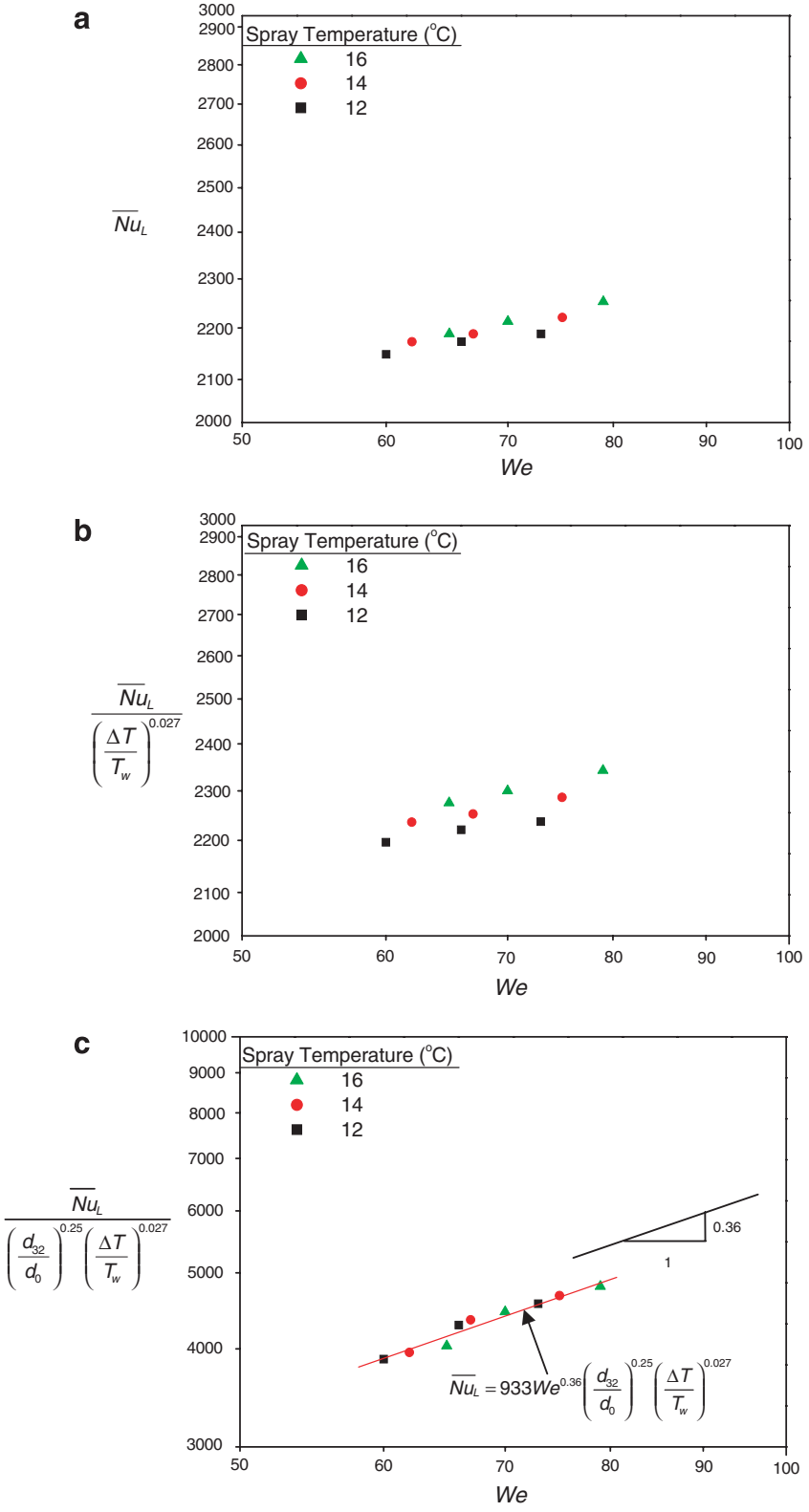

Fig. 8. The correlation of $\overline{Nu}_L$ on We, d_{32}/d_0, and $\Delta T/T$.

never found as one would expect because the present R-134a spray has strong coherent flow structure and greater spray interactions than those of a conventional jet. The velocity decreases as the spray travels downstream may be caused by the several reasons. The major reason is due to the atomization process, which results in a distribution of drop sizes and velocities. Small drops tend to move slower, because they have a higher surface-to-volume ratio and consequently higher drag [18]. The other reasons are not clearly understood at this stage. However, it is certain that this definitely cannot be only factor responsible for the observed reductions in the jet centerline velocity along the downstream. The impact velocity was also plotted in Fig. 5. Although the measurements were not easy, the results look reasonable and good. Due to different Re_j and We, the values of the present study are different from those of Yoshida et al. a bit [19]. However, they also have the same trend. Fig. 6 shows the correlations based on the results of the present study (R-134a) with those from Tien [20] (water). It is found that the dimensionless centerline spray velocity $u^*(u_o/u_e)$ was a function of the dimensionless downstream distance z^* $(=z/H)$ and We. Weber number dependence is clearly observed.

4.5. Spray impingement heat transfer

Spray data were taken as a function of R-134a mass flux G for three different spray liquid temperatures in terms of ΔT $(=T_s - T_l)$. Unlike Oliphant et al. [12], the dependence of average heat transfer coefficients on Weber number at three spray liquid temperatures of 12, 14, and 16 °C was studied and is shown in Fig. 7 at a fixed $z = 90$ mm. It indicates that a higher heat transfer removal rate was found with a spray at larger mass flux (i.e. large We). Following Oliphant et al. [12], this may be caused by the combination of high surface area evaporation cooling and "unsteady" nature of a boundary layer forming due to droplet impact on the impingement surface. Generally, the heat removal rate was found to be about 0.06–0.12 MW/m^2.

The data shown in Fig. 7 also indicate that a lower spray liquid temperature result in higher heat transfer rates (e.g. 12 °C). However, based on the definition of $\bar{h}$, the heat transfer coefficients decrease as ΔT increases. Based on the preceding flow visualization, larger but fewer droplets occur at lower temperatures due to an increase in surface tension at lower temperatures. The heat transfer mechanisms for the heat removal rate of the present spray impingement on surfaces at temperatures lower than the normal boiling temperature of the liquid may consist of the following components: a component due to the sensible heating (e.g. ΔT for the present study) of the thermal boundary layer as it forms in a relatively thin, rapidly moving radially outward film; a convective component due to discrete and random nature of the droplet arrival creates a mixing effect; and unsteady interface between the very thin liquid layer and the spray entrainment air provides effective evaporation cooling. The above three factors are competed and counteracted on heat removal. An increase in the liquid flow rate would result in a thicker film as evidenced by Fig. 2. This would decrease evaporation and convective heat transfer due to a larger thermal resistance. However, an increase in liquid flow also results in an increase in convective heat transfer to the liquid. Since the variations in G were not significant, the influence due to the mass flux seems not noted.

The data of Fig. 8(a)–(c) suggest that the heat transfer may correlate with the Weber number We, the number takes into account the spray dynamics, d_{32}/d_0 describes

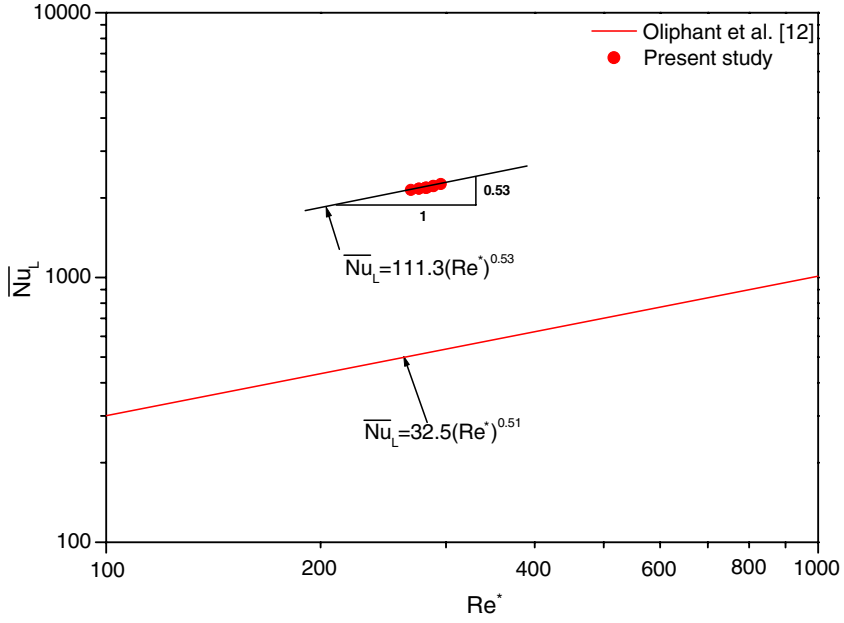

Fig. 9. Comparison of the present study with those of previous study.

the droplet size effect, and $\Delta T/T_s$ stands for the dimensionless temperature illustrating the effect of sensible heating. The correlation was plotted in Fig. 8(a)–(c). The coefficients and powers of the terms of We, d_{32}/d_0, and $\Delta T/T_s$ are 933, 0.36, 0.25, and 0.027, respectively for R-134a. $\overline{Nu}_L$ was calculated based on the heat flux along the center and the side length (L) of the target plate and represents an ensemble average. This composite correlation can finally be expressed in the following form:

$$\overline{Nu}_L = 933We^{0.36}(d_{32}/d_0)^{0.25}(\Delta T/T_s)^{0.027} \quad (5)$$

This more accurate correlation was developed to account for the variations in droplet impact velocity in terms of We, size distribution, d_{32}/d_0, and sensible heat effect on heat transfer. It is found that, the powers of first two terms strongly suggest that the influence of droplet hydrodynamics and droplet parameters on heat removal are significant. In fact, such results can clearly be seen in Fig. 8(a). This is perhaps due to the present liquid spray with a high frequency of droplet impingement upon the target surface as evidenced by Fig. 2, leaving much of the surface covered with fairly stagnant liquid (see Fig. 2 for details) with a relatively thick film. This may explain why Weber number (i.e. volumetric flux) is of a little greater significance to characterize spray heat transfer than droplet size and other parameters as reported in Estes and Mudawar [21]. It is also found that the correlation can predict 80% of data within $\pm 10\%$. Finally, the present results were plotted and compared with those of previous studies [12] as shown in Fig. 9. It was found the power of Re^* seems the same with different magnitude as one would expect. In fact, the present $\overline{Nu}_L$ are higher than those of [12].

5. Conclusion

A series of experiments were conducted with LDV and thermal measurements as well as optical visualization on the effect of different spray mass flux in terms of We, and other relevant parameters. It was found that We has a strong effect on spray velocity characteristic and droplet size distribution as well as local Sauter mean diameter while in-flight. So does the heat removal rate. The spray becomes more uniform at high volumetric flux in terms of We and further downstream as well. The spray atomization mechanisms and droplet evolution were examined and discussed. The experimental data show that a significant reduction in droplet diameter was found due to both fragmentation and evaporation of R-134a sprays. Thickness for spray impingement have been observed and measured to be 0.93–1.35 mm of the present study. The heat transfer coefficient was found to increase with ΔT and mass flux G in the present non-boiling regime. Furthermore, the heat removal rate was found to be strongly Weber number and (d_{32}/d_0) dependent. Finally, a composite correlation illustrating the above-stated relevant parameters is developed.

References

[1] B.E. Gelfand, Droplet breakup phenomena in flows with velocity lag, Progr. Energy Combust. Sci. 22 (1996) 201–265.
[2] N. Ashgriz, R. Washburn, T. Barbat, Segregation of drop size and velocity in jet impinging splash-plate atomizers, Int. J. Heat Fluid Flow 17 (1996) 509–516.
[3] D.W. Stanton, C.J. Rutland, Multi-dimensional modeling of thin liquid films and spray-wall interactions resulting from impinging sprays, Int. J. Heat Mass Transfer 41 (1998) 3037–3054.
[4] A. Kuffenath, B. Wende, W. Leuckel, Influence of liquid flow conditions on spray characteristics of internal-mixing twin-fluid atomizers, Int. J. Heat Fluid Flow 20 (1999) 513–519.
[5] B.M. Pikkula, J.H. Torres, J.W. Tunnell, B. Anvari, Cryogen spray cooling: effects of droplet size and spray density on heat removal, Laser Surgery Med. 28 (2001) 103–112.
[6] R.D. Ingebo, Atomization of liquid sheets in high pressure air flow, NASA TM-83731, NASA-Lewis Researcher Center, Cleveland, OH, 1984.
[7] M.M. Elkotb, Fuel atomization for spray modeling, Progr. Energy Combust. Sci. 8 (1982) 61–91.
[8] Y. Zhou, S. Lee. McDonell, S. Samuelsen, R.L. Kozarek, E.J. Lavernia, Influence of operating variables on average droplet size during linear atomization, Atomization Sprays 7 (1997) 358–393.
[9] R.D. Ingebo, Characteristics of vaporizing cryogenic sprays for rocket combustion modeling, NASA Technical Memorandum 106615. 4004966696, 1994.
[10] K.J. Choi, S.C. Yao, Mechanism of film boiling heat transfer of normally impacting sprays, Int. J. Heat Mass Transfer 30 (1987) 311–318.
[11] S.C. Yao, K.J. Choi, Heat transfer experiments of monodispersed vertically impacting sprays, Int. J. Multiphase Flow 13 (1987) 639.
[12] K. Oliphant, B.W. Webb, M.Q. McQuay, An experimental comparison of liquid jet array and spray impingement cooling in the non-boiling regime, Exp. Therm. Fluid Sci. 18 (1998) 1–10.
[13] S.-S. Hsieh, T.-C. Fan, H.-H. Tsai, Spray cooling characteristics of water and R-134a, Part I. Nucleate boiling, Int. J. Heat Mass Transfer 47 (2004) 5703–5712.
[14] S.-S. Hsieh, T.-C. Fan, H.-H. Tsai, Spray cooling characteristics of water and R-134a, Part II. Transient cooling, Int. J. Heat Mass Transfer 47 (2004) 5713–5724.
[15] K.M. Graham, E. Ramadhyani, Experimental and theoretical studies of mist jet impingement cooling, ASME J. Heat Transfer 118 (1996) 343–349.
[16] S.-S. Hsieh, P.-J. Chan, H.-J. Chin, Turbulent flow in a rotating two pass smooth channel, ASME J. Fluids Eng. 121 (1999) 725–734.
[17] B. Horacek, K.T. Kiger, J. Kim, Single nozzle-spray cooling heat transfer mechanisms, Int. J. Heat Mass Transfer 48 (2005) 1425–1438.
[18] M. Orme, Experiments on droplet collision, bounce, coalescence and disruption, Progr. Energy Combust. Sci. 23 (1997) 65–79.
[19] K. Yoshida, Y. Abe, T. Oka, Y.H. Mori, A. Nagashima, Spray condition under reduced gravity condition, ASME J. Heat Transfer 123 (2001) 309–318.
[20] C.-H. Tien, Droplet size and velocity of a water spray, MS Thesis, Department of Mechanical and ElectroMechanical Engineering, National Sun Yat-Sen University, 2005 (in Chinese).
[21] K.A. Estes, I. Mudawar, Correlation of Sauter mean diameter and critical heat flux for spray cooling of small surfaces, Int. J. Heat Mass Transfer 38 (1995) 2985–2996.